

Probing Primordial Magnetic Fields Using Ly α Clouds

Kanhaiya L. Pandey¹ AND Shiv K. Sethi¹

Received _____; accepted _____

arXiv:1210.3298v2 [astro-ph.CO] 27 Oct 2012

¹Raman Research Institute, Bangalore 560080, India

ABSTRACT

From previous studies of the effect of primordial magnetic fields on early structure formation, we know that the presence of primordial magnetic fields during early structure formation could induce more perturbations at small scales (at present $1\text{--}10 h^{-1}\text{Mpc}$) as compared to the usual ΛCDM theory. Matter power spectrum over these scales are effectively probed by cosmological observables such as shear correlation and Ly α clouds, In this paper we discuss the implications of primordial magnetic fields on the distribution of Ly α clouds. We simulate the line of sight density fluctuation including the contribution coming from the primordial magnetic fields. We compute the evolution of Ly α opacity for this case and compare our theoretical estimates of Ly α opacity with the existing data to constrain the parameters of the primordial magnetic fields. We also discuss the case when the two density fields are correlated. Our analysis yields an upper bounds of roughly $0.3\text{--}0.6$ nG on the magnetic field strength for a range of nearly scale invariant models, corresponding to magnetic field power spectrum index $n \simeq -3$.

Subject headings: Cosmology: primordial magnetic field, Ly α clouds, structure formation

1. Introduction

In the past 10 years, cosmological weak lensing and the study of Ly α clouds in the redshift range $2 \lesssim z \lesssim 5$ have emerged as reliable methods to precisely determine the matter power spectrum on scales below $10 h^{-1}\text{Mpc}$. In particular, these methods can estimate the matter power spectrum at small scales which are not directly accessible to other methods e.g. galaxy surveys (for details and further references see e.g. Munshi et al. (2008); Hoekstra & Jain (2008); Croft et al. (1998, 1999, 2002)).

Large scale magnetic fields been observed in galaxies and clusters of galaxies with the coherence lengths up to $\simeq 10\text{--}100$ kpc (for a review see e.g. Widrow (2002)). There is also some evidence of coherent magnetic fields up to super-cluster scales (Kim et al. 1989). These fields play an important role in various astrophysical processes. Still little is known about the origin of large scale cosmic magnetic fields, and their role in the evolutionary history of the universe. These fields could have originated from dynamo amplification of very tiny seed magnetic fields $\simeq 10^{-20}$ G (e.g Parker (1979); Zeldovich, Ruzmaikin & Sokolov (1983); Ruzmaikin, Sokolov & Shukurov (1988)). It is also possible that much larger primordial magnetic fields ($\simeq 10^{-9}$ G) were generated during the inflationary phase (Turner & Widrow 1988; Ratra 1992) and the large scale magnetic field observed today are the relics of these fields. These large scale primordial fields could be directly detected by upcoming and future radio interferometers such as LOFAR and SKA (for details see e.g. www.lofar.org and www.skatelescope.org/pages/page_sciencegen.htm).

The impact of large scale primordial magnetic fields on CMBR temperature and polarization anisotropies has been studied in detail (e.g. Subramanian & Barrow (1998B, 2002); Seshadri & Subramanian (2001); Mack et al. (2002); Lewis (2004); Gopal & Sethi (2005); Tashiro & Sugiyama (2006); Sethi & Subramanian (2005); Sethi et al. (2008); Sethi & Subramanian (2009); Sethi, Haiman, Pandey (2010); Kahniashvili & Ratra (2005); Giovannini & Kunze (2008); Yamazaki et al. (2008); Seshadri & Subramanian (2009);

Trivedi et al. (2010, 2012)). Wasserman (1978) demonstrated that primordial magnetic fields can induce density perturbations in the post-recombination universe. Further work along these lines have investigated the impact of this effect for the formation of first structures, reionization of the universe, and the signal from redshifted HI line from the epoch of reionization (e.g. Kim et al. 1996; Gopal & Sethi 2003; Sethi & Subramanian 2005; Tashiro & Sugiyama 2006; Schliecher, Banerjee, Klessen 2009; Sethi & Subramanian 2009). The matter power spectrum induced by primordial magnetic fields can dominate the matter power spectrum of the standard Λ CDM model at small scales. Probes such as cosmological weak gravitational lensing can directly probe this difference and therefore reveal the presence of primordial fields and put additional constraint on their strength Pandey & Sethi (2012).

In this paper we attempt to constrain primordial magnetic fields within the framework of the distribution of Ly α clouds in the IGM in the redshift range $2 \lesssim z \lesssim 5$. These clouds have been shown to originate in the mildly non-linear density regions of the IGM (Cen & Ostriker (1994)). This has allowed development of detailed semi-analytic methods to understand the observed properties of these clouds (e.g. Bi et al. 1995; Hui et al. 1997; Choudhury et al. 2001a,b). Adopting a semi-analytic approach, we simulate density fluctuation along the line of sight, including the contribution of matter perturbations induced by these magnetic fields. We compute effective Ly α opacity of the IGM for this computed Ly α cloud distribution and compare our results with the existing data (e.g. Faucher-Giguère et al. 2008).

In the previous analyses, the density perturbations induced by magnetic fields are assumed to be uncorrelated to the density field generated by the usual Λ CDM model. Recently, Caldwell & Motta (2011) showed that if the conformal invariance of electromagnetism is broken during the inflation and thus produced the primordial magnetic fields, these magnetic fields may be correlated with the primordial density perturbations.

In our analysis we have made a separate case for such fields.

Throughout the paper, we used flat ($k=0$) Λ CDM universe with $\Omega_m = 0.24$, $\Omega_b = 0.044$, $h = 0.73$ and $\sigma_8 = 0.77$.

2. Primordial Magnetic Field And Induced Matter Power Spectrum

In the primordial theory of the magnetic fields, it is postulated that the large scale primordial magnetic fields of strengths $\simeq 10^{-9}$ G were present in the very early universe; these fields could have originated during the inflation. They are assumed to be tangled magnetic fields which can be characterized by a power-law power spectrum: $M(k) = Ak^n$. In the prerecombination era, the magnetic fields are dissipated at scales below a scale corresponding to $k_{\max} \simeq 200 \times (10^{-9} \text{ G}/B_{\text{eff}})$ (Jedamzik, Katalinić, & Olinto 1998; Subramanian & Barrow 1998A, e.g.). Here B_{eff} is the RMS at this cut-off scale for a given value of the spectral index, n . Another possible normalization, commonly used in the literature, is the value of RMS at $k = 1 \text{ Mpc}^{-1}$, B_0 . These two normalizations are related as: $B_{\text{eff}} = B_0 k_{\max}^{(n+3)/2}$. It is possible to present results using either of the pair $\{B_{\text{eff}}, n\}$ or $\{B_0, n\}$.

The PMF induced matter perturbations grow in the post recombination era by gravitational instability. The matter power spectrum of these perturbations is given by: $P(k) \propto k^{2n+7}$, for $n < -1.5$, the range of spectral indices we consider here (Wasserman 1978; Kim et al. 1996; Gopal & Sethi 2003).

Magnetic field induced matter perturbations can only grow for scales above the magnetic field Jean's length: $k_J \simeq 15 \times (10^{-9} \text{ G}/B_{\text{eff}})$ (e.g. Kim et al. 1996; Kahniashvili et al. 2010). The dissipation of tangled magnetic field in the post-recombination era also results in an increase in the thermal Jeans length (Sethi & Subramanian 2005; Sethi et al. 2008). For

most of the range of magnetic field strengths and the physical setting (Lyman- α clouds at a temperature of $\simeq 10^4$ K) considered here, the scale corresponding to k_J generally are comparable to or smaller than the thermal Jeans length.

For our computation, we need to know the time evolution of the matter power spectrum induced by tangled magnetic fields. It can be shown that the dominant growing mode in this case has the same time dependence as the Λ CDM model (see e.g. Gopal & Sethi (2003) and references therein)

3. The Simulation: Density Fluctuation Along The Line of Sight: Distribution of Ly α Clouds

We describe a brief outline of the numerical simulation in this section. Hydrodynamical simulations have shown that Ly- α clouds are mildly non-linear ($\delta \lesssim 10$) regions of the IGM at high redshifts. This allows one to analytically derive important observables from the Lyman- α clouds semi-analytically, in terms of a few parameters denoting the ionization, thermal, and dynamical state of the clouds.

Here we have closely followed the semi-analytic prescription given in Bi & Davidson (1997). In this paper we have considered two cases of primordial magnetic field induced matter perturbations : (a) pure Λ CDM matter perturbations and primordial magnetic field (PMF) induced matter perturbations are uncorrelated (b) those two are correlated. In both cases we compute two separate line of sight density (and velocity) fields each corresponding to a single kind of matter perturbations. In the former case, these fields are drawn from different realizations and in the latter the fields are generated from the same realization. We add these two density (and velocity) fields to get the final density (and velocity) fields in the IGM. To simulate line of sight IGM density and velocity fields for a given three dimensional matter power spectrum (inflationary/PMF induced), first we calculate the

corresponding three dimensional baryon power spectrum, which corresponds to the original power spectrum smoothed over the scales below the larger of the thermal or Magnetic Jeans scale x_b

$$P_B^{(3)}(k, z) = \frac{P_{\text{DM}}^{(3)}(k, z)}{[1 + x_b^2(z)k^2]} \quad (1)$$

where

$$x_b(z) = \frac{1}{H_0} \left[\frac{2\gamma k_B T_m(z)}{3\mu m_p \Omega_m (1+z)} \right]^{1/2} \quad (2)$$

then we compute one dimensional baryon (density, velocity and density-velocity) power spectra, which will be used in the further computation. We note here that the relevant scale of smoothing for the range of magnetic field values and the IGM temperatures we consider is thermal Jeans scale and not the magnetic Jeans scale. The one-dimensional power spectra can be computed using the following relations

$$P_B^{(1)}(k, z) = \frac{1}{2\pi} \int_{|k|}^{\infty} dk' k' P_B^{(3)}(k, z) \quad (3)$$

$$P_v^{(1)}(k, z) = \dot{a}^2(z) k^2 \frac{1}{2\pi} \int_{|k|}^{\infty} \frac{dk'}{k'^3} P_B^{(3)}(k, z) \quad (4)$$

$$P_{Bv}^{(1)}(k, z) = i\dot{a}(z) k \frac{1}{2\pi} \int_{|k|}^{\infty} \frac{dk'}{k'} P_B^{(3)}(k, z) \quad (5)$$

where a is the scale factor.

The density ($\delta_0(k, z)$) and velocity ($v(k, z)$) fields in one dimension are two correlated Gaussian random fields (the correlation is given by the density-velocity power spectrum), we use inverse Gram-Schmidt procedure to simulate them in terms of two independent Gaussian random fields $w(k)$ and $u(k)$ of power spectra respectively $P_w(k)$ and $P_u(k)$

$$\delta_0(k, z) = D(z)[u(k) + w(k)] \quad (6)$$

$$v(k, z) = F(z)i\dot{a}k\beta(k, z)w(k, z) \quad (7)$$

where $D(z)$ and $F(z)$ are the linear density and velocity growth factors. Functions $\beta(k)$, $P_w(k)$ and $P_u(k)$ are function of $P_B^{(3)}(k)$,

$$\beta(k, z) = \int_{|k|}^{\infty} \frac{P_B^{(3)}/k'^3 dk'}{P_B^{(3)}/k' dk'} \quad (8)$$

$$P_w(k) = \frac{1}{\beta(k)} \int_{|k|}^{\infty} \frac{P_B^{(3)}(k')}{k'} dk' \quad (9)$$

$$P_u(k) = \frac{1}{2\pi} \int_{|k|}^{\infty} P_B^{(3)}(k') k' dk' - P_w(k) \quad (10)$$

We compute $\delta_0(k, z)$ and $v(k, z)$ for both kinds of perturbations separately, the corresponding $\delta_B(x, z)$ and $v(x, z)$ is computed by using Fourier transforms. And then we add the contribution from both the kinds together ($\delta_B(x, z) = \delta_B^{\text{infl}}(x, z) + \delta_B^{\text{pmf}}(x, z)$ and $v(x, z) = v^{\text{infl}}(x, z) + v^{\text{pmf}}(x, z)$) to get the final combined line of sight density and velocity fields. To compute one dimensional density field for the pmf induced perturbations we use the three-dimensional matter power spectrum (e.g. Gopal & Sethi, 2003); for inflationary perturbations we use the standard Λ CDM power spectrum.

For our computations we have generated the density and velocity fields for 25 redshift bins between the redshifts 0 to 5. In each bin we have 2^{14} points resolving the Jeans scale by at least a factor of 4. The cutoff scale (Jeans scale, x_b) is the larger of the thermal Jeans length and the magnetic Jeans length.

To take into account the non-linearity of density perturbations in the IGM we use lognormal distribution of the IGM density field Bi & Davidson (1997), thus the number density of baryons in IGM is taken to be,

$$n_B(x, z) = A e^{\delta_B(x, z)} \quad (11)$$

A is a constant which can be determined using following relation,

$$\langle n_B(x, z) \rangle \equiv n_0(z) = A \langle e^{\delta_B(x, z)} \rangle \quad (12)$$

since $\delta_B(x, z)$ is a Gaussian random variable,

$$\langle e^{\delta_B(x, z)} \rangle = e^{\langle \delta_B^2(x, z) \rangle} \quad (13)$$

thus

$$n_B(x, z) = n_0(z) e^{(\delta_B(x, z) - \langle \delta_B^2(x, z) \rangle)} \quad (14)$$

where $n_0(z)$ is the background baryon number density given by,

$$n_0(z) = \frac{\Omega_B \rho_c}{\mu_B m_p} (1 + z)^3 \quad (15)$$

4. Calculation of Ly α opacity

The optical depth τ is given by

$$\tau(\nu) = \int n_{\text{HI}}(t) \sigma_a \left(\frac{\nu}{a} \right) dt \quad (16)$$

where n_{HI} is number density of neutral hydrogen in the IGM, ν is the observed frequency, which is related to redshift z by $z \equiv (\nu_a/\nu) - 1$, ν_a is the Ly α frequency at rest. The absorption cross section σ_a is given by,

$$\sigma_a = \frac{I_a}{b\sqrt{\pi}} V \left(\alpha, \frac{\nu - \nu_a}{b\nu_a} + \frac{v}{b} \right) \quad (17)$$

where parameter $b = (2kT/m_p)^{1/2}$ is the velocity dispersion and $v(x)$ is the peculiar velocity field, $\alpha \equiv 2\pi e^2 \nu_a / 3m_e c^3 b = 4.8548 \times 10^{-8}/b$, $I_a = 4.45 \times 10^{-18} \text{cm}^{-2}$ and V is the Voigt function.

The number density of neutral hydrogen, n_{HI} can be computed by solving ionization equilibrium equation,

$$n_{\text{HI}}(x, z) = \frac{\alpha[T(x, z)]n_{\text{B}}(x, z)}{\alpha[T(x, z)] + \Gamma_{\text{ci}}[T(x, z)] + J(z)/[\mu_e n_{\text{B}}(x, z)]} \quad (18)$$

where $T(x, z)$ is given by $T(x, z) = T_0(z)[n_{\text{B}}(x, z)/n_0(z)]^{\gamma-1}$ where $T_0(z)$ is the temperature of the IGM at the mean density and γ is the polytropic index for the IGM; γ captures the dynamical state of the IGM gas which gives rise to the observed Lyman- α absorption. These parameters are likely to take values in the ranges $4000 \lesssim T_0 \lesssim 15,000$ K and $1.3 \lesssim \gamma \lesssim 1.6$ (Hui & Gnedin, 1997). $\alpha(T)$, $\Gamma_{\text{ci}}(T)$ and $J(z)$ are recombination rate, collisional ionization rate and photo ionization rates in the IGM. For temperature $T \simeq 10^4$ K, the combination of these effects yields (Croft et al. 1998),

$$\tau(z) \propto n_{\text{B}}^2 T^{-0.7} = A(n_{\text{B}}/n_0)^{2-0.7(\gamma-1)},$$

$$A = 0.946 \left(\frac{1+z}{4}\right)^6 \left(\frac{\Omega_{\text{B}} h^2}{0.0125}\right)^2 \left(\frac{T_0}{10^4 \text{K}}\right)^{-0.7} \left(\frac{J}{10^{12} \text{s}^{-1}}\right)^{-1} \left[\frac{H(z)}{H_0}\right]^{-1} \quad (19)$$

To compare with the data we have computed effective optical depth which is the observable quantity in the form of decrease in observed flux ($F \propto e^{-\tau}$) and is given by,

$$\tau_{\text{eff}}(z) = -\log [\langle \exp(-\tau) \rangle] \quad (20)$$

The data which we have used for comparison with simulation results has been obtained using high resolution spectral observations like HIRES, ESI and MIKE having FWHM in the range of 6–44 km sec⁻¹ (Faucher-Giguère et al. (2008)), which resolve the Jeans scales over the redshifts we are considering. Since we are also resolving Jeans scale in our simulation, we can directly compare our theoretical results with this data without taking into account the scale dependence of τ_{eff} in our analysis.

The mean opacity $\langle \tau \rangle$ and the effective opacity are computed by averaging over all the realizations of τ for a given redshift bin.

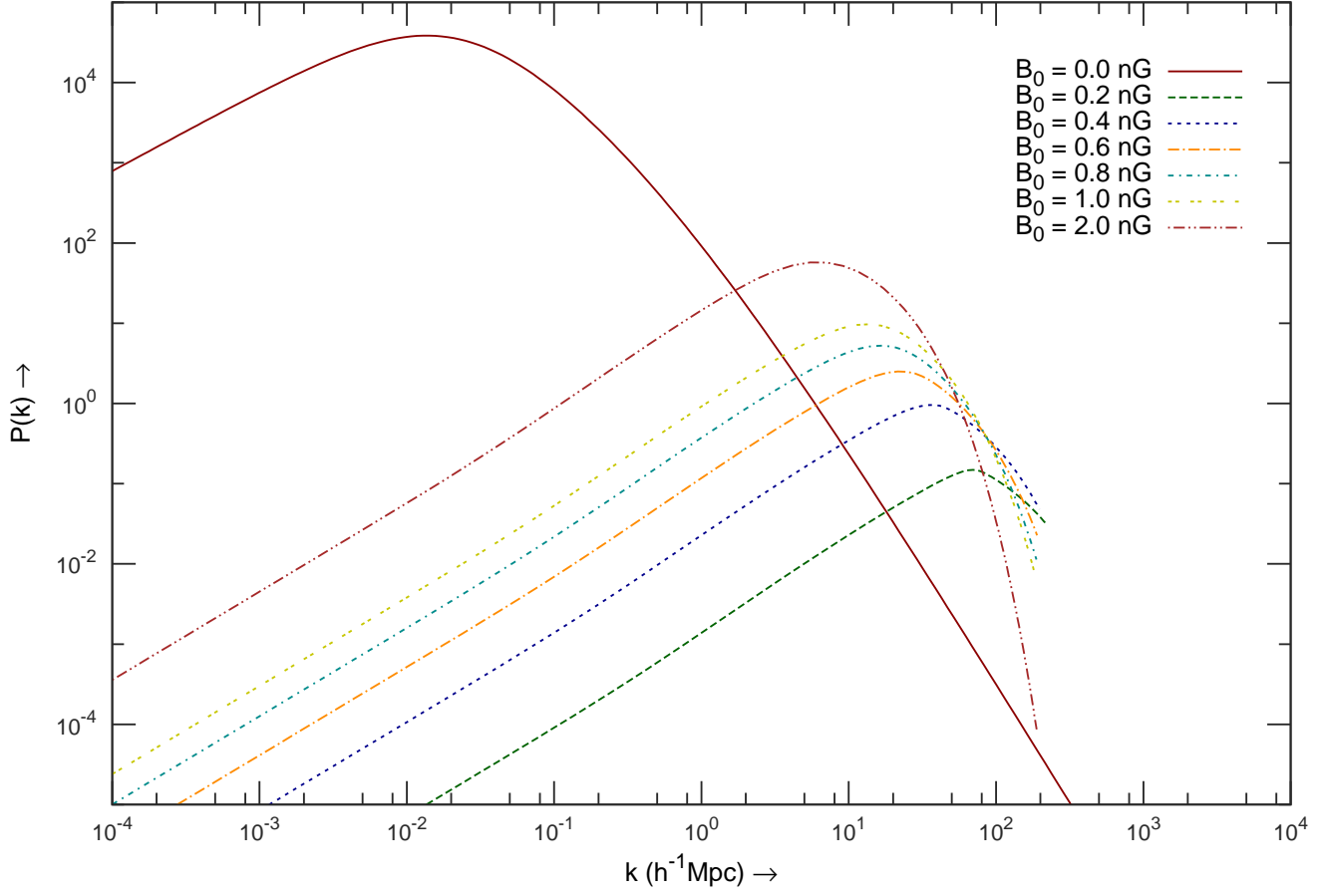


Fig. 1.— The matter power spectrum for magnetic case, with added exponential cutoff and then smoothed around magnetic Jeans length k_J , is displayed for various values of magnetic field strength B_0 . Spectral index n is -2.95 for each case. Along with that the red curve is matter power spectrum for pure Λ CDM non-magnetic case.

5. Results

In Figure 1 we show the matter power spectra at the present epoch for magnetic case, along with the pure Λ CDM (non-magnetic) matter power spectrum, which has been used in our calculations, here an exponential cut-off around k magnetic Jeans scale is assumed. This figure shows that the magnetic field induced matter power spectra can dominate over the pure Λ CDM case at small scales ($k \geq 1$ h/Mpc). The effect of this excess has already been studied in the context of early structure formation, reionization, and weak-lensing signals (Sethi & Subramanian (2005, 2009), Pandey & Sethi (2012)) As an extension to that body of work we explore the effect of this excess on Ly α effective opacity in this paper.

In Figure 2 we show the variation of Ly α opacity $\langle\tau\rangle$ with redshift for various values of magnetic field strengths. The red dots with y-errorbars are the observed values of Ly α opacity τ_{eff} (Faucher-Giguère et al. (2008)). It should be pointed out that the inclusion of peculiar velocities in the computation of τ (Eq. (17)) makes a negligible difference to the value of either average or effective opacity.

Figure 1 corresponds to the case when matter perturbations induced by primordial magnetic fields and the inflationary matter perturbations are not correlated. The average opacity $\langle\tau\rangle$ is not an observable quantity. The aim of Figure 2 is to demonstrate that the inclusion of PMF matter perturbations enhances the average opacity of the IGM.

In Figure 3 we show the variation of τ_{eff} with redshift for various values of magnetic field strength along with the observed evolution of τ_{eff} . This plot is for the case when matter perturbations induced by primordial magnetic field and the inflationary matter perturbations are not correlated. Comparing this figure with Figure 2 we see that the slope of redshift evolution of τ_{eff} is far smaller than for average opacity. This difference is owing to the fact that for HI column densities $N_{\text{HI}} \gtrsim 10^{14} \text{ cm}^{-2}$, the optical depth exceeds one. For column densities larger than this saturation value, the optical depth increases only as

logarithm of the column density and therefore these clouds get a smaller weight in the the computation of τ_{eff} . As the average opacity of the IGM increases sharply with increasing redshift (Eq. (19)), this effect is more enhanced at higher redshifts.

A comparison between Figures 2 and 3 shows that an increase in $\langle\tau\rangle$ doesn't necessarily lead to an increase in τ_{eff} . In Figure 3 it is seen that τ_{eff} is greater than the usual ΛCDM case for $z \lesssim 3$ but falls below the predictions of this model for larger redshifts.

We can understand this behaviour by the following set of arguments. The change in the effective optical depth $d\tau_{\text{eff}} \propto \sum_i \exp(-\tau_i)d\tau_i$, where τ_i refers to optical depths of individual clouds. On the other hand, $d\langle\tau\rangle \propto \sum_i d\tau_i$. As seen in Figure 2, the inclusion of PMF density perturbations increase $\langle\tau\rangle$ or $\sum_i d\tau_i > 0$, but $\sum_i \exp(-\tau_i)d\tau_i$ could be negative if $d\tau_i$ is negative wherever τ_i is smallest. To elaborate this point, In Figure 6 we have plotted the distribution of optical depths τ_i s for the 1.5 nG case ($z = 4$), against the $d\tau_i = \tau_i (2 \text{ nG}) - \tau_i (0 \text{ nG}); (z = 4)$. It is clear from this figure that τ_i values are small when $d\tau_i$ is more negative, or this can make $\sum_i \exp(-\tau_i)d\tau_i$ negative, and thus it explains the decrease of τ_{eff} even when there is increase in $\langle\tau\rangle$ with increasing magnetic field values. It should be pointed out that this behaviour of τ_{eff} cannot be mimicked by a change in J , γ (Eq. (19)) or by a scaling of the power spectrum by changing the value of σ_8 .

The Figure 4 and Figure 5 are for the same analysis as Figure 2 and Figure 3 respectively, but for the case when induced matter perturbations and inflationary matter perturbations are correlated. In Figure 4 the values of $\langle\tau\rangle$ are smaller in comparison to the corresponding values in the case of uncorrelated matter perturbations.

For detailed comparison with observations we performed the likelihood analysis for the τ_{eff} against the Faucher-Giguère et al. (2008) data as a function of four parameters, J ((1.4 to 2.0) 10^{-12}), γ (1.4 to 2.0), B_0 ((0.1 to 2.0) nG), and n (-2.80 to -2.99). To compute the posterior probability for magnetic field parameters, we marginalized the likelihood function

over the parameters J & γ . Figure 7 shows the results of this analysis for the uncorrelated case. The curves from top to bottom are the contours for 5σ , 3σ and 1σ levels for a range of $\Delta\chi^2 = \chi_i^2 - \chi_{\min}^2$. We see that in this case for $n = -2.90$ the allowed values (by 5σ) of magnetic field are $B_0 < 0.6-0.7$ nG, and for $n = -2.95$ is $B_0 < 1.3$ nG.

In Figure 8, we compare this result with our previous analysis with the weak-lensing data Pandey & Sethi (2012) and the present analysis with the correlated case: the lower triplet (red green and blue), solid and dashed corresponds to the uncorrelated and the correlated cases respectively of the present analysis, whereas the upper triplet (dotted) correspond to our previous analysis with the weak-lensing data. It is clearly seen from Figure 8 that the constraints arising from the correlated case are not very different from the uncorrelated case. Or the Lyman- α clouds do not provide an appropriate physical setting for distinguishing between these two cases. From Figure 8 it also follows that our present constraints are considerably stronger than our previous analysis with the cosmological weak-lensing data.

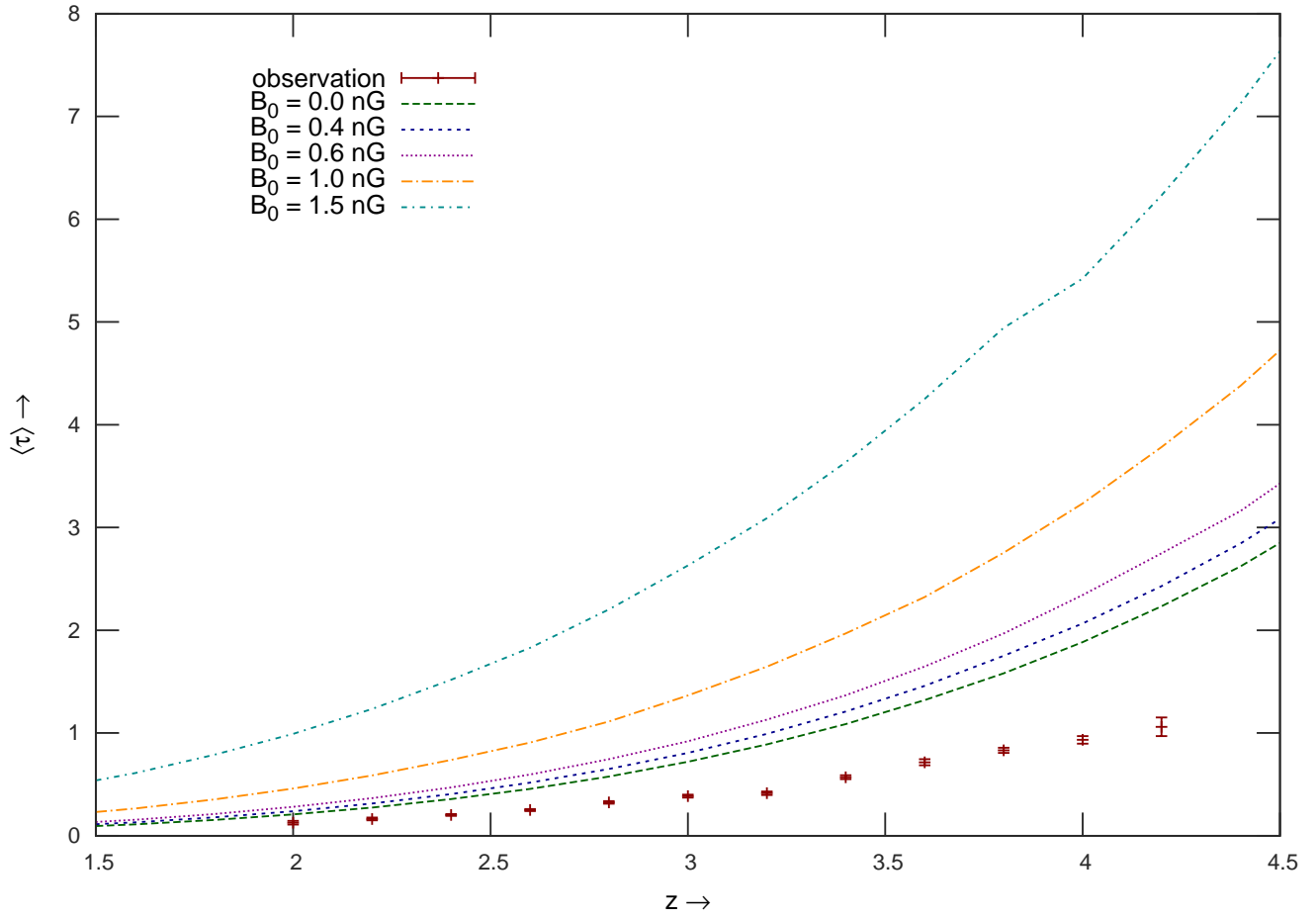


Fig. 2.— The evolution of Ly α opacity $\langle \tau \rangle$ for the magnetic and non magnetic cases, uncorrelated δ_{infi} and δ_{pmf} case.

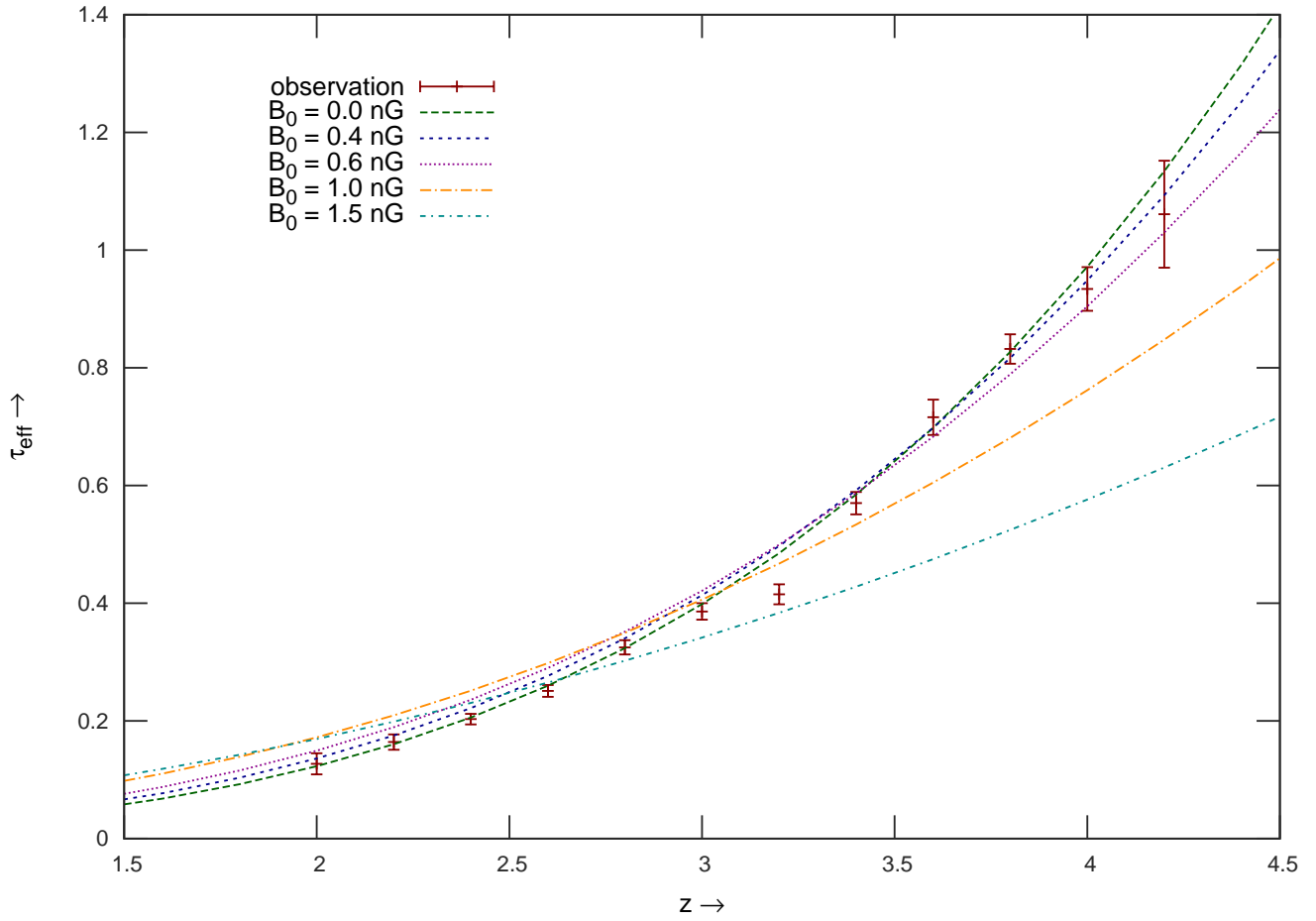


Fig. 3.— The evolution of Ly α opacity τ_{eff} for the magnetic and non magnetic cases, uncorrelated δ_{infi} and δ_{pmf} case.

6. Discussion

Primordial tangled magnetic fields leave their signatures on cosmological observables for a large range of scales from sub-Mpc to 10^4 Mpc. CMBR temperature and polarization anisotropies provide probes for the magnetic fields for scales $\gtrsim 10$ Mpc (e.g. Kahniashvili et al. 2010). Recently, Yamazaki et al. (2010) computed the allowed region in the $\{B_0, n\}$ plane by comparing the predictions of primordial magnetic field models with existing CMBR observations. Constraints on smaller scale come from early formation of structures induced by PMF. The observables that impact these scales include early reionization, HI signal from the epoch of reionization (Sethi & Subramanian (2009, 2005), Schleicher & Miniati (2011)), cosmological weak gravitation lensing (Pandey & Sethi (2012)), etc. Other constraints on large scale cosmological magnetic fields arise from rotation measure of high redshift polarized radio sources (e.g. Kolatt 1998; Sethi 2003; Blasi et al. 1999); rotation measure (RM) of radio sources will be one of the methods employed by radio interferometers LOFAR and SKA to attempt to detect cosmic magnetic fields. In particular, Blasi et al. (1999) considered the same physical setting (high redshift Lyman- α clouds) as in this paper. They computed the RM of Ly α density field and obtained bounds $\simeq 10^{-8}$ G on magnetic fields with coherence length scales of the thermal Jeans length.

In addition to the upper bounds on the magnetic field strength obtained by these observables, recent results suggests that there might be a lower bound of $\simeq 10^{-15}$ G on the magnetic field strength (e.g. Dolag (2010); Neronov & Vovk (2010); Tavecchio et al. (2010); Taylor et al. (2011)). Another lower bound is obtained from the study of echo emission from the blazar Mrk 501 (Takahashi et al. (2012)) which suggests magnetic field strength of $B_0 \gtrsim 10^{-20}$ G coherent over the length scale of ~ 1 kpc. This would suggest that the magnetic field strength could lie in the range $10^{-20} < B_0 < \text{a few } 10^{-9}$ G. This range is still too large for a better determination of the magnetic field strength.

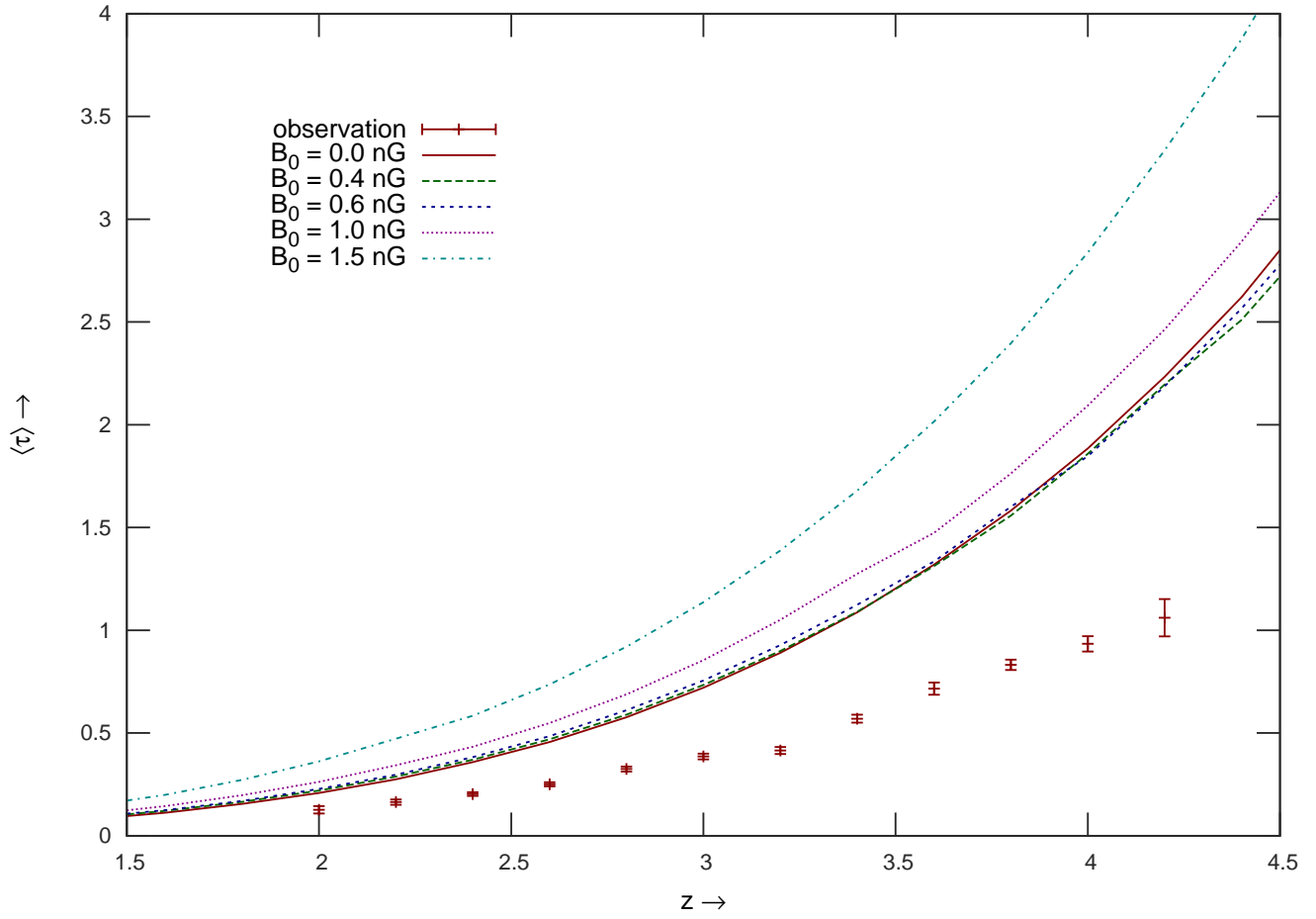


Fig. 4.— The evolution of Ly α opacity $\langle \tau \rangle$ for the magnetic and non magnetic cases, correlated δ_{inff} and δ_{pmf} case.

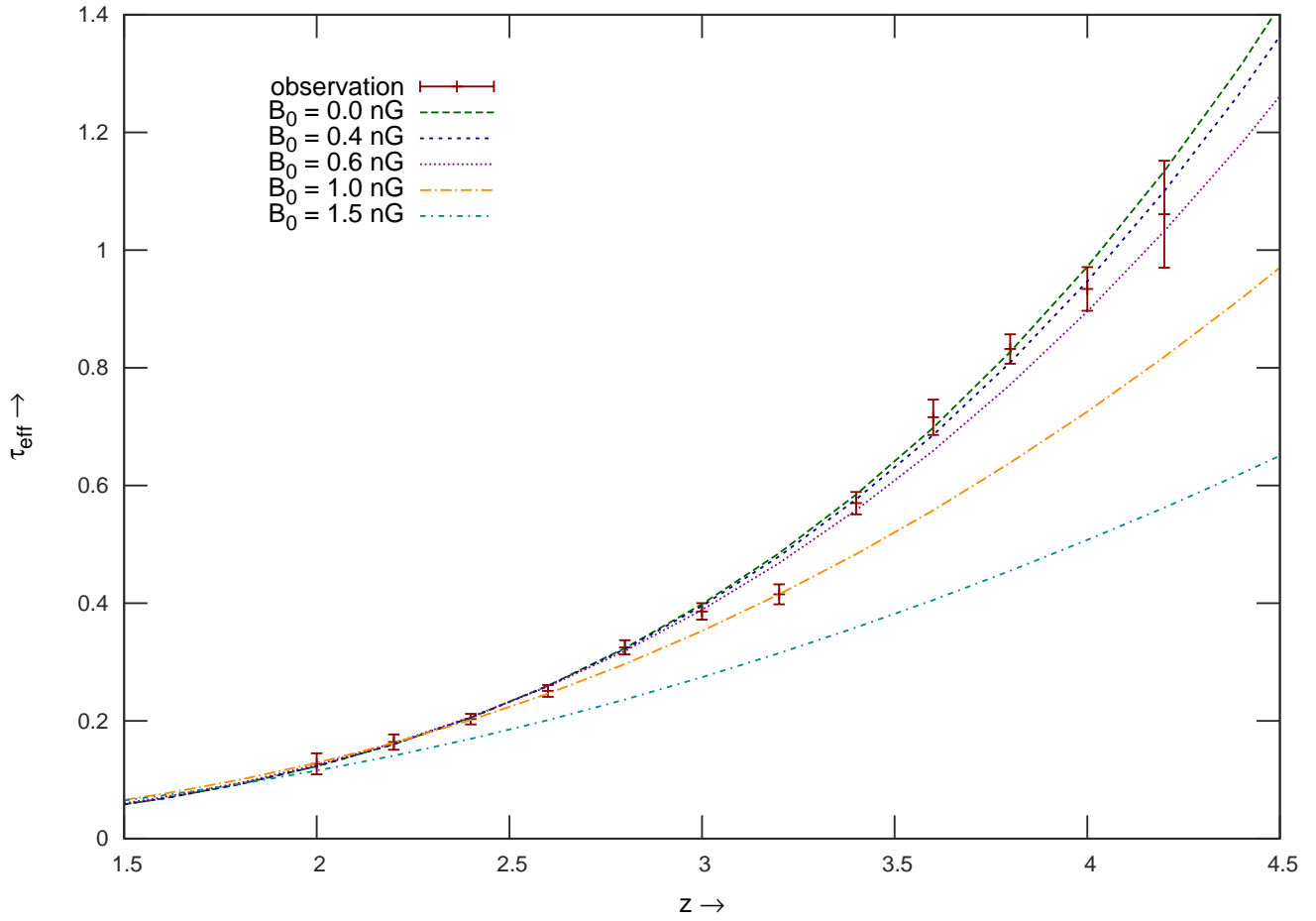


Fig. 5.— The evolution of Ly α opacity τ_{eff} for the magnetic and non magnetic cases, correlated δ_{inff} and δ_{pmf} case.

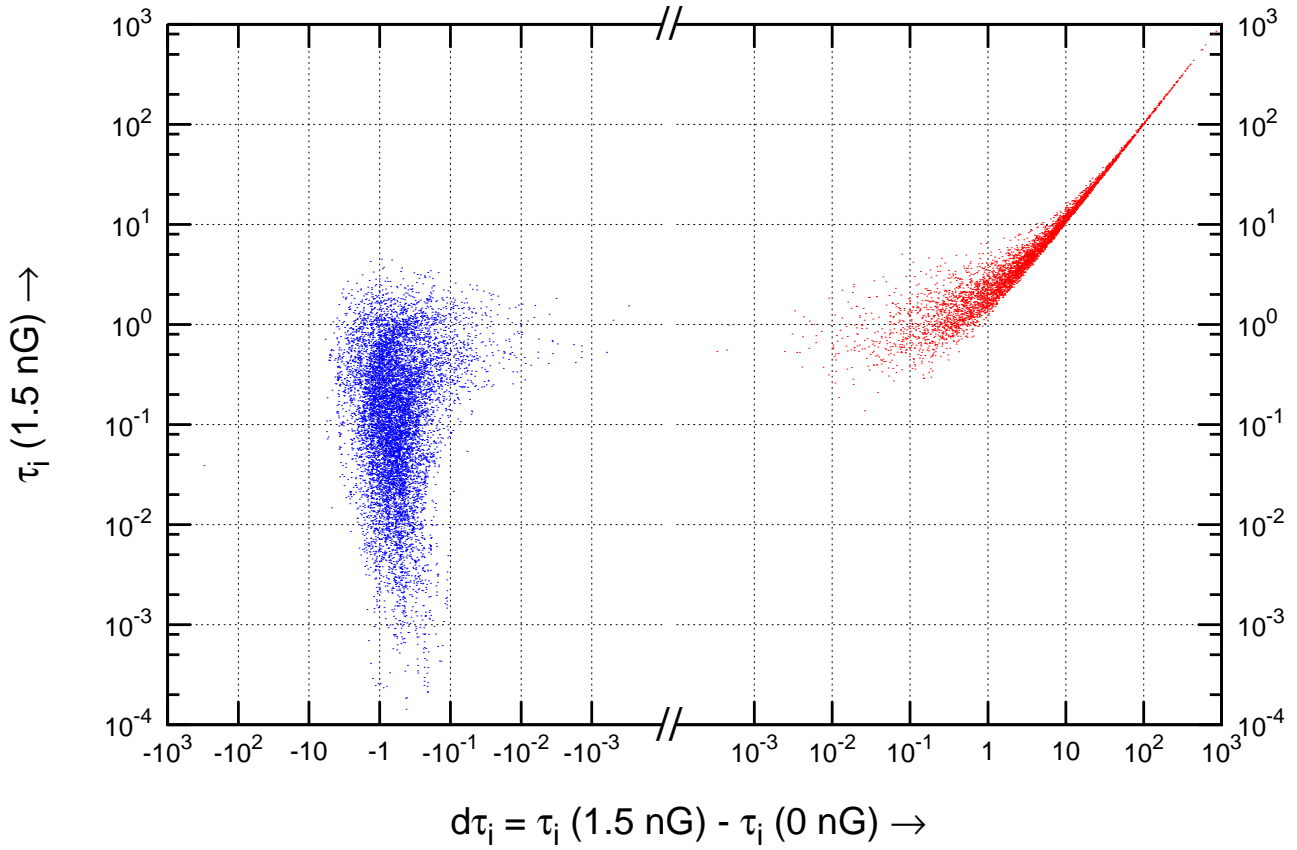


Fig. 6.— The distribution of $\tau_i (1.5 \text{ nG})$ versus $d\tau_i (= \tau_i (1.5 \text{ nG}) - \tau_i (0 \text{ nG}))$ at redshift $z = 4$.

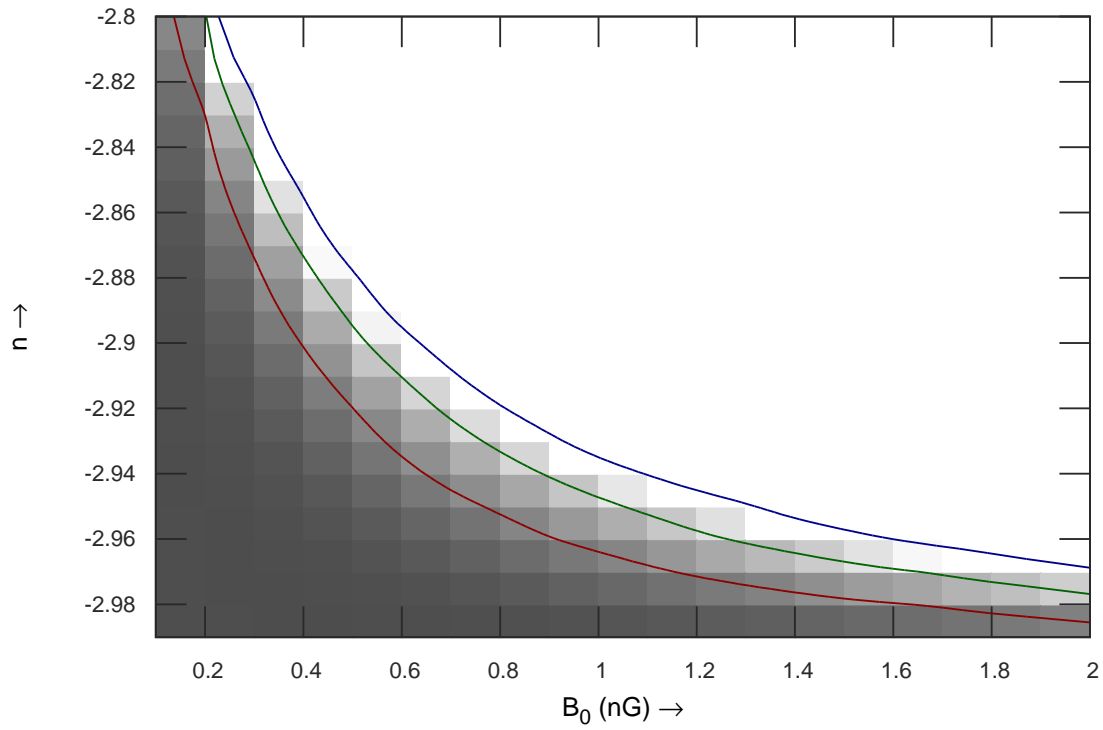


Fig. 7.— Allowed (the shaded) region in the (B_0, n) plane, based on the χ^2 analysis of τ_{eff} against the data from Faucher-Giguère et al. (2008). The three curves (from top to bottom) are contours at the 5σ , 3σ and 1σ levels.

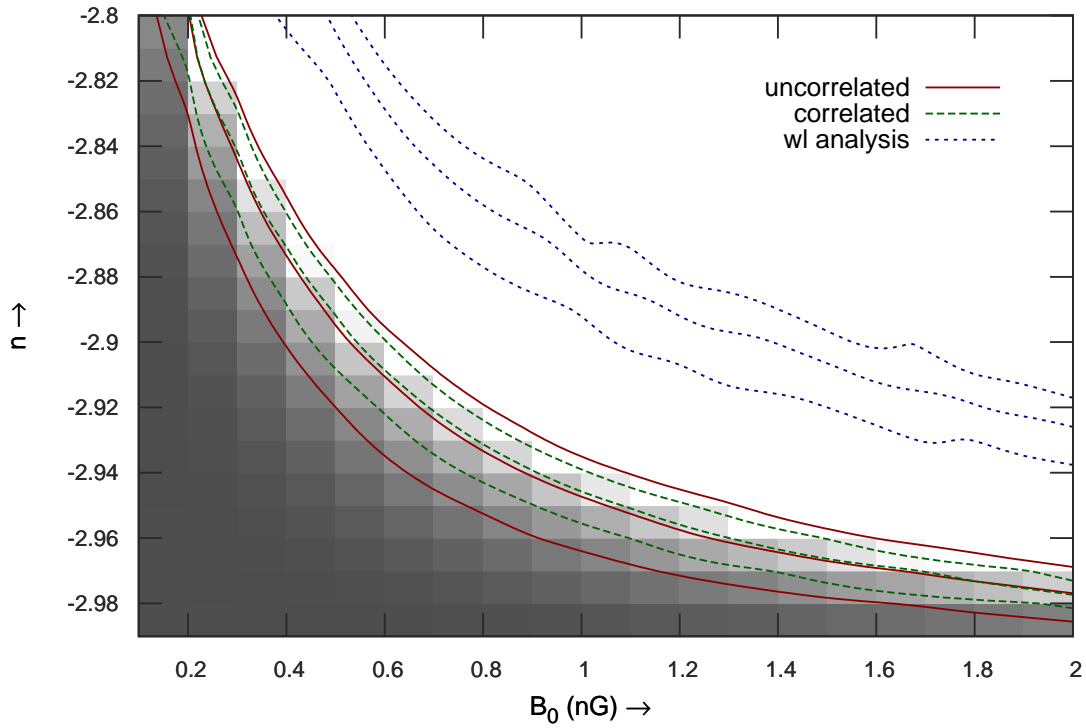


Fig. 8.— Contour of $\Delta\chi^2 = \chi_i^2 - \chi_{\min}^2$ for the present analysis (the lower triplets, solid ones correspond to 1, 3 and 5 sigma levels for the uncorrelated case, the dashed ones are the same for the correlated case) and the previous analysis (the upper triplet) on (B_0, n) plane.

In Figure 7, we show the constraints from the present study compare with similar constraints from cosmological gravitational lensing we obtained earlier (Pandey & Sethi (2012)). In Comparison to bounds on primordial magnetic fields from CMBR anisotropies (e.g. Figure 1 of Yamazaki et al. (2010)), for the entire range of spectral indices, we obtain stronger limits on B_0 . Other constraints from bispectrum and trispectrum analysis of CMBR passive scalar modes Trivedi et al. (2010, 2012) are 2.4 nG and 0.7 nG, they have used spectral index value $n = -2.8$, whereas for $n = -2.8$ our analysis gives an upper bound on $B_0 \lesssim 0.3$ nG (Figure 7). As noted above, these bounds are even better than our previous analysis with the weak-lensing data (Figure 8).

In our present analysis, we consider four parameter: J , γ , B_0 , n but no other cosmological parameters. We also do not account for errors arising from different realizations of the density field. Our current bounds can be further improved by the inclusion of such effects. We note that even though the magnetic field signal could be degenerate with the overall normalization of the Λ CDM model as measured by σ_8 , the current errors on the value of σ_8 (WMAP 7-year data give $\sigma_8 = 0.801 \pm 0.030$ (Larson et al. 2011)) are too small to sufficiently alter our conclusions.

In sum: Lyman- α clouds provide a sensitive probe of the matter power spectra at scales $\lesssim 1$ Mpc. Primordial magnetic field induced matter perturbations give additional power at these scale which can be probed using the redshift evolution of τ_{eff} . Our results shows that this leads to one of the most stringent bounds on the parameters of primordial magnetic fields. These bounds can be further improved by more data on the evolution of τ_{eff} at low redshifts and also more precise data at higher redshifts. Recently, Becker et al. (2012) have provided a measurement of the evolution τ_{eff} which is in agreement with the data we have used (Faucher-Giguère et al. (2008)) for our analysis but claims better precision. In future, similar analyses with such data can give even more stringent constraints on the parameters of primordial magnetic fields.

Acknowledgement

We thank R Srianand and S Sridhar on many useful discussions on many aspects of this paper.

REFERENCES

- Becker, G. D., Hewett, P. C., Worseck, G., & Prochaska, J. X. 2012, arXiv:1208.2584
- Bi, H., Ge, J., & Fang, L.-Z. 1995, ApJ, 452, 90
- Bi, H., Davidson, Arthur F. 1997, ApJ497, 523
- Blasi, P., Burles, S., & Olinto, A. V. 1999, ApJ, 514, L79
- Cen, R., & Ostriker, J. P. 1994, ApJ, 431, 451
- Coles, P., & Jones, B. 1991, MNRAS, 248, 1
- Croft, R. A. C., Weinberg, D. H., Katz, Neal et al. 1998, ApJ, 495, 44
- Croft, R. A. C., Weinberg, D. H., Pettini, Max et al. 1999, ApJ, 520, 1
- Croft, R. A. C., Weinberg, D. H., Bolte, M., et al. 2002, ApJ, 581, 20
- Caldwell, Robert R. & Motta, Leonardo 2011, Phys. Rev. D, 84, 123525
- Choudhury, T. R., Srianand, R., & Padmanabhan, T. 2001, ApJ, 559, 29
- Choudhury, T. R., Padmanabhan, T., & Srianand, R. 2001, MNRAS, 322, 561
- Dolag, K. 2010, Highlights of Astronomy, 15, 461
- Faucher-Giguère, C.-A., Prochaska, J. X., Lidz, A., Hernquist, L., & Zaldarriaga, M. 2008, ApJ, 681, 831
- Giovannini, M. & Kunze, K. E. 2008, Phys. Rev. D, 77, 063003.
- Gopal, R. & Sethi, S. K. 2003, J. Astrophys. Astron., 24, 51
- Gopal, R. & Sethi, S. K. 2005, Phys. Rev. D72, 103003

- Hoekstra, H., & Jain, B. 2008, *Annual Review of Nuclear and Particle Science*, 58, 99
- Hui, L., Gnedin, N. Y., & Zhang, Y. 1997, *ApJ*, 486, 599
- Jedamzik, K., Katalinić, V., & Olinto, A. V. 1998, *Phys. Rev. D*, 57, 3264
- Kahniashvili, Tina; Ratra, Bharat 2005, *Phys. Rev. D*, 71, 103006.
- Kahniashvili, Tina; Tevzadze, Alexander G.; Sethi, Shiv K.; Pandey, Kanhaiya; Ratra, Bharat 2011, *Phys. Rev. D*, 82, 083005
- Kim, E., Olinto, A. V., Rosner, R. 1996, *ApJ*, 468, 28.
- Kim, K. T., Kronberg, P. P., Giovannini, G., Venturi, T. 1989, *Nature*, 341, 720.
- Kolatt, T. 1998, *ApJ*, 495, 564
- Larson, D., Dunkley, J., Hinshaw, G., et al. 2011, *ApJS*, 192, 16
- A. Lewis, *Phys. Rev. D*. 70, 43011, 2004
- Mack, A., Kahniashvili, T., Kosowsky, A. 2002, *Phys. Rev. D*, 65, 123004.
- Munshi, D., Valageas, P., van Waerbeke, L., & Heavens, A. 2008, *Phys. Rep.*, 462, 67
- Neronov, A., & Vovk, I. 2010, *Science*, 328, 73
- Pandey, Kanhaiya L. & Sethi, Shiv K. 2012, *ApJ*, 748, 1
- Parker, E. N. 1979, *Cosmical Magnetic Field: Their Origin and Their Activity*, (Oxford University Press).
- Ratra, B. 1992, *ApJL*, 391, L1.
- Ruzmaikin, A. A., Sokolov, D. D., Shukurov, A. M. 1988, Moscow, Izdatel'tvo Nauka, 1988, 280 p.

Schleicher, D. R. G., Banerjee, R., Klessen R. S. 2009, ApJ, 692, 236

Schleicher, D. R. G., & Miniati, F. 2011, MNRAS, 418, L143

Seshadri, T. R., Subramanian, K. 2001, Phys. Rev. Lett.87, 101301.

Seshadri, T. R., Subramanian, K. 2009, Phys. Rev. Lett.103, 081303.

Sethi, S. K. 2003, MNRAS, 342, 962

Sethi, S. K., Subramanian, K. 2005, MNRAS, 356, 778.

Sethi, S. K., Nath, B. B., Subramanian, K. 2008, MNRAS, 387, 1589.

Sethi, S. K., Subramanian, K. 2009, JCAP, 11, 21.

Sethi, Shiv, Haiman, Zoltan, Pandey, Kanhaiya 2010, ApJ, 721, 615.

Subramanian, K. & Barrow, J. D. 1998, Phys. Rev. D, 58, 83502

Subramaniyan, K., Barrow, J. D. 1998, Phys. Rev. Lett., 81, 3575.

Subramaniyan, K., Barrow, J. D. 2002, MNRAS, 335, L57.

Takahashi, K., Mori, M., Ichiki, K., Inoue, S. 2012, ApJ, 744, L7.

Tashiro, H., Sugiyama, N. 2006, MNRAS, 368, 965.

Tavecchio, F., Ghisellini, G., Foschini, L., et al. 2010, MNRAS, 406, L70

Taylor, A. M., Vovk, I., & Neronov, A. 2011, A&A, 529, A144

Trivedi, Pranjal, Subramaniyan, K., Seshadri, T. R. 2010, Phys. Rev. D, 82, 123006

Trivedi, Pranjal, Seshadri, T. R., Subramaniyan, K. 2012, Phys. Rev. Lett., 108, 23

Turner, M. S., Widrow, L. M. 1988, PRD, 37, 2743.

Wasserman, I. 1978, ApJ, 224, 337.

Widrow, L. M. 2002, Reviews of Modern Physics, 74, 775.

Yamazaki, D. G., Ichiki, K., Kajino, T., Mathews, G. J. 2008, Phys. Rev. D, 2008, 77,
043005

Yamazaki, D. G., Ichiki, K., Kajino, T., Mathews, G. J. 2010, Advances in Astronomy,
2010, 586590

Zeldovich, I. B., Ruzmaikin, A. A., Sokolov, D. D. 1983, The Fluid Mechanics of
Astrophysics and Geophysics. Volume 3, (New York: Gordon and Breach Science
Publishers), 381 p.